Aerodynamic Estimation Techniques for Aerostats and Airships

S. P. Jones*
TCOM Corporation, Columbia, Maryland
and
J. D. DeLaurier†
University of Toronto, Toronto, Canada

A semiempirical steady-state model of a finned axisymmetric body is developed and used to compute hull-fin mutual interference factors and cross-flow drag coefficients from wind tunnel data on five aerostats and airships. The results are in general agreement with expectations from theory and provide a basis for predicting aerodynamic coefficients. The model is extended to unsteady motion by considering the local flow on finite hull segments and the fins. This dynamic model is applicable to nonlinear simulations and the computation of rotational stability derivatives for which equations are derived. Rotational stability derivatives calculated from static wind tunnel data agree well with experimental data from a rotating-arm tow tank if convective acceleration terms are included in the calculations.

Introduction

THE motivation for this research came from the need to accurately represent an aerostat's or airship's aerodynamic forces and moments in flight-dynamic analyses, such as stability calculations and nonlinear simulation. This article presents a cross-flow analytical model for finned axisymmetric bodies, which are traditionally LTA-vehicle configurations. The model permits analysis of static wind tunnel data to obtain empirical factors to account for mutual hull-fin interference, and provides a means of computing forces and moments when the vehicle is in dynamic motion.

This analysis draws much from the work of earlier researchers; the representation of the hull's axially distributed forces by local geometry and cross flow was initially based on Munk's[1] normal-force potential-flow equations for airships. The formulation currently used was a later development by Allen and Perkins[2] which additionally accounted for axial forces and viscosity. This is used in the steady-state aerodynamic representation described in the next section. For unsteady motion, additional terms need to be included, such as apparent-mass effects. Jones'[3] equations for an arbitrary body undergoing general motions in inviscid fluid show the way in which these effects integrate to give forces and moments. This provided the basis for the present representation of the hull's unsteady-force distribution, as described later.

For the fins' contribution, it was found that previous research was not adequate to accurately predict the mutual hull-fin interference effect. The wing-fuselage work of Multhopp[4] assumed dominance of the wing's aerodynamics over the fuselage's, and the finned-missile work of Nielsen[5] assumed very slender, low-aspect-ratio fins. Modern LTA designs have hull-fin configurations which are between these two extremes, and the present work takes a semiempirical approach where hull-fin interference factors are defined in the analytical model, and obtained from experimental data as functions of certain geometrical parameters. This approach is similar to that of DeLaurier and Podleski,[6] which used Munk's hull equations; but the present analytical model is much refined from this earlier work.

Steady-State Analytical Model

The analytical model is schematically represented in Fig. 1 where it is divided into two distinct aerodynamic regions: the hull, which extends from the nose to the hull-fin intersection point, l_h, and the fins, which continue from that point to their trailing edge. For nonseparated flow, the hull forces and moment are obtained from Allen and Perkins,[2] and the fins' normal force is obtained from Wardlaw,[7] with efficiency factors η_k and η_f introduced to account for mutual interference between the hull and fins. This then gives the following equations: normal force,

$$N = q_0\{(k_3 - k_1)\eta_k I_1 \sin(2\alpha)\cos(\alpha/2) + (Cd_c)_h \sin\alpha\sin|\alpha| J_1 + S_f[(Cn^*_\alpha)_f \eta_f (\sin(2\alpha)/2) + (Cd_c)_f \sin\alpha\sin|\alpha|]\} \quad (1)$$

axial force,

$$D = q_0\{[(Cd_h)_0 S_h + (Cd_f)_0 S_f]\cos^2\alpha - (k_3 - k_1)\eta_k I_1 \sin(2\alpha)\sin(\alpha/2) - (Ct)_f S_f\} \quad (2)$$

moment (about the nose),

$$M_{\text{nose}} = -q_0[(k_3 - k_1)\eta_k I_3 \sin(2\alpha)\cos(\alpha/2) + (Cd_c)_h J_2 \sin\alpha\sin|\alpha| + S_f\eta_f (l_f)_1 (Cn^*_\alpha)_f (\sin(2\alpha)/2) + S_f (l_f)_2 (Cd_c)_f \sin\alpha\sin|\alpha|] \quad (3)$$

where

q_0 = steady-state dynamic pressure $= \rho U_0^2/2$
α = steady-state angle of attack
k_1, k_3 = axial and lateral apparent-mass coefficients, respectively (see Ref. 1)
η_k = hull-efficiency factor accounting for the effect of the fins on the hull

Presented as Paper 81-1339 at the AIAA Lighter-than-Air Systems Conference, Annapolis, Md., July 8-10, 1981; submitted July 21, 1981; revision received Feb. 19, 1982.

*Advisory Scientist. Member AIAA.
†Associate Professor, Institute for Aerospace Studies.

$(Cd_c)_h$ = hull cross-flow drag coefficient, referenced to J_1
$(Cd_c)_f$ = fins cross-flow drag coefficient, referenced to S_f
$(Cn^*_\alpha)_f$ = derivative of the isolated fins normal force coefficient with respect to α, at $\alpha=0$ and referenced to S_f
η_f = fin-efficiency factor accounting for the effect of the hull on the fins
$(Cd_h)_0$ = hull zero-angle axial drag coefficient, referenced to S_h
$(Cd_f)_0$ = fins zero-angle axial drag coefficient, referenced to S_f
$(Ct)_f$ = fins leading-edge suction coefficient, referenced to S_f
S_f = fins reference area
S_h = hull reference area
$(l_f)_1$ = distance from the hull nose to the fins aerodynamic center
$(l_f)_2$ = distance from the hull nose to the fins center of cross-flow force

Also,

$$I_1=\int_0^{l_h}\frac{dA}{d\xi}d\xi=A_h \qquad I_3=\int_0^{l_h}\xi\frac{dA}{d\xi}d\xi$$

$$J_1=\int_0^{l_h}2r d\xi \qquad J_2=\int_0^{l_h}2r\xi d\xi$$

where A is the hull cross-sectional area; ξ is the axial distance along the hull, from the nose; and r is the hull radius.

These equations may be made nondimensional by the definitions:

$$N,D=(Cn,Cd)q_0S$$

$$M=Cmq_0S\bar{C}$$

$$I_1,J_1,S_f,S_h=(\hat{I}_1,\hat{J}_1,\hat{S}_f,\hat{S}_h)S$$

$$I_3,J_2=(\hat{I}_3,\hat{J}_2)S\bar{C}$$

$$(l_f)_1,(l_f)_2=[(\hat{l_f})_1,(\hat{l_f})_2]\bar{C}$$

where S is the vehicle reference area (hull volume)$^{2/3}$, and $\bar{C}$ is the vehicle reference length, total hull length.

Also, it was assumed that the α magnitudes for attached flow are less than 30 deg. Hence $\cos(\alpha/2)\simeq 1$, and Eqs. (1-3) become

$$Cn=[(k_3-k_1)\eta_k\hat{I}_1+0.5(Cn^*_\alpha)_f\eta_f\hat{S}_f]\sin(2\alpha)+[(Cd_c)_h\hat{J}_1+(Cd_c)_f\hat{S}_f]\sin\alpha\sin|\alpha| \quad (4)$$

$$Cd=[(Cd_h)_0\hat{S}_h+(Cd_f)_0\hat{S}_f]\cos^2\alpha-(k_3-k_1)\eta_k\hat{I}_1\sin(2\alpha)\sin(\alpha/2)-(Ct)_f\hat{S}_f \quad (5)$$

$$(Cm)_{nose}=-[(k_3-k_1)\eta_k\hat{I}_3+0.5(\hat{l_f})_1(Cn^*_\alpha)_f\eta_f\hat{S}_f]\sin(2\alpha)-[(Cd_c)_h\hat{J}_2+(Cd_c)_f(\hat{l_f})_2\hat{S}_f]\sin\alpha\sin|\alpha| \quad (6)$$

For the application of these equations to a given configuration, note that the integrals $\hat{I}_1$, $\hat{J}_1$, $\hat{I}_3$, $\hat{J}_2$ may be readily calculated from the hull geometry. Also, the apparent-mass coefficients, k_1 and k_3, may be obtained from Munk,[1] as functions of the hull fineness ratio. However, the fins' geometry requires further definitions, where the planform is chosen to be that shown as area S_f in Fig. 2. With this, plus the airfoil properties, $(Cn^*_\alpha)_f$ and $(\hat{l_f})_1$ may be found from finite-wing methods such as described by Etkin[8] and Lowry and Polhamus.[9]

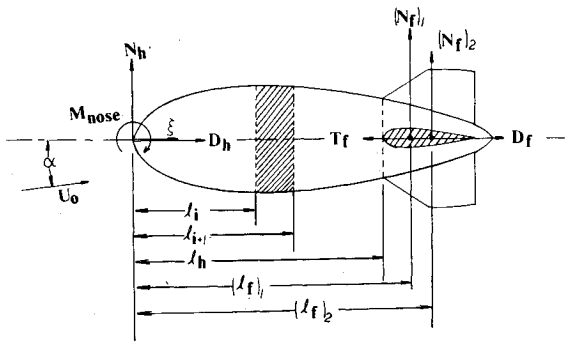

Fig. 1 Schematic of steady-state analytical model.

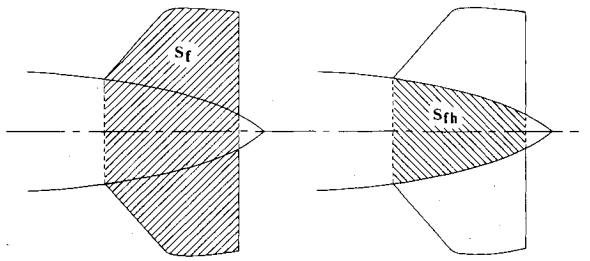

Fig. 2 Fin planform definition.

Wardlaw[7] presents graphs by which one may find $(Cd_c)_h$ and $(Cd_c)_f$. In particular, $(Cd_c)_h$ is chosen to be the cross-flow drag coefficient of a circular cylinder at the hull's maximum cross-flow Reynolds number. He also gives a correction factor for this as a function of the bare-hull's fineness ratio; but, as the experimental results will show, this may not be suitable for a finned hull.

The $(Cd_c)_f$ values are for sharp-edged fins, and are plotted as functions of aspect ratio and taper ratio. The semiempirical results to be presented indicate that these may also be appropriate for fins with rounded leading edges and the planform S_f in Fig. 2. However, the results also show that $(\hat{l_f})_2$ is best chosen at the area center of the exterior portion of the fins, that is, with reference to Fig. 2, area S_f-S_{fh}.

For the axial drag coefficients, $(Cd_h)_0$ and $(Cd_f)_0$, these may be found in a variety of ways, including the methods documented by Hoerner.[10] Also, the fins leading-edge suction coefficient $(Ct)_f$ may be calculated from

$$(Ct)_f=(Cn^*_\alpha)_f\eta_f\eta_t\frac{\sin(2\alpha)}{2}\tan\alpha-\frac{[(Cn^*_\alpha)_f\eta_f\sin(2\alpha)]^2\eta_t}{4\pi(AR)_f} \quad (7)$$

where the first term on the right-hand side represents the action by the leading edge to bring the airfoil circulation-lift vector normal to the mean flow, in accordance with the Blasius theorem. This action is modified, though, by the actual efficiency of the leading edge, η_t, which is affected by Reynolds number and geometry. Some representative values for η_t are given by Putman et al.[11] Note that $\eta_t=0$ for sharp leading edges. The second term represents the attenuation of leading-edge suction due to the wing's finite aspect ratio. Traditionally, this has also been associated with a tilting of the circulation-lift vector, through the concept of "induced drag."

Parameter Determination From Wind Tunnel Data

Remaining to be determined are the efficiency factors, η_k and η_f. If it is assumed that these factors as well as the cross-flow drag coefficients, $(Cd_c)_h$ and $(Cd_c)_f$, remain constant

with α (a considerable mathematical convenience), Eqs. (4) and (6) provide a means of computing all four parameters from experimental wind tunnel data. The normal-force and moment equations can be written in the form

$$Cn = a_1 \sin(2\alpha) + b_1 \sin\alpha \sin|\alpha| \tag{8}$$

$$(Cm)_{\text{nose}} = a_2 \sin(2\alpha) + b_2 \sin\alpha \sin|\alpha| \tag{9}$$

The coefficients a_i and b_i can be determined by curve fitting experimental data to Eqs. (8) and (9). Sufficient information is then available to calculate empirical values of the parameters.

$$\eta_k = \frac{a_1(\hat{l}_f)_1 + a_2}{(k_3 - k_1)[\hat{I}_1(\hat{l}_f)_1 - \hat{I}_3]} \tag{10}$$

$$\eta_f = \frac{a_1\hat{I}_3 + a_2\hat{I}_1}{0.5(Cn^*_\alpha)_f \hat{S}_f[\hat{I}_3 - \hat{I}_1(\hat{l}_f)_1]} \tag{11}$$

$$(Cd_c)_h = \frac{b_1(\hat{l}_f)_2 + b_2}{\hat{J}_1(\hat{l}_f)_2 - \hat{J}_2} \tag{12}$$

$$(Cd_c)_f = \frac{b_1\hat{J}_2 + b_2\hat{J}_1}{\hat{S}_f[\hat{J}_2 - \hat{J}_1(\hat{l}_f)_2]} \tag{13}$$

Experimental data on a number of airships and aerostats have been analyzed by this procedure. In particular, the data used came from wind tunnel tests on models of TCOM aerostats by Gove and Haak,[12] airships ZR-1 (Zahm et al.[13]) and ZRS-4 (Freeman[14]) by NACA, and a University of Washington "Class C" aerostat by Peters et al.[15] These by no means exhaust all available test data on airships and aerostats, but they best meet the criteria of giving accurate values as well as precisely defining the model geometries.

The force and moment coefficients were obtained from the tabulated and plotted values. The other parameters, calculated as previously described, are given in Table 1. From these, a least-squares fit of the analytical model with the data gave values for η_k, η_f, $(Cd_c)_h$, and $(Cd_c)_f$ which are given in Table 2.

The interference or efficiency factors are plotted in Fig. 3. The factor η_f is plotted as a function of S_{fh}/S_f, the degree to which the fins are covered by the hull (see Fig. 2). Note that η_f should equal unity when S_{fh}/S_f equals zero (fins alone) and equal zero when $S_{fh}/S_f = 1$ (no fins). The data show a fairly uniform trend between these two extremes.

It was assumed that η_k is a function of the ratio of the effective fin area to the hull's complete projected area. For vehicles with conventional cruciform tails this ratio is $S_f/(J_1)_{\text{tot}}$. The University of Washington aerostat, however, was equipped with a vee tail, the horizontal stabilizer having a dihedral angle, $\Gamma = 30$ deg. The vertical aerodynamic force on an airfoil having a dihedral angle, Γ, is proportional to $S_f\cos^2(\Gamma)$.[16] Therefore the independent variable for η_k was taken to be $S_f\cos^2(\Gamma)/(J_1)_{\text{tot}}$. When the latter is zero (no fins), η_k should equal unity and increase with relative fin size because of the upwash ahead of the fins. This upwash increases the flow angle on a portion of the body immediately ahead of the fins, in the manner described by Multhopp[4] for wings on fuselages. Because $dA/d\xi < 0$ on this portion, the pitching moment of the body is increased. This should be manifested by an increase of η_k, as, in fact, is seen in the data. The η_k increase may also be interpreted as an increase in the body's effective fineness ratio.

The intention of this least-squares matching was to obtain curves for η_k and η_f, as in Fig. 3, thus completing the information needed for the application of this model to the aerodynamic estimations of finned axisymmetric bodies. However, the cross-flow drag results for the example airships provided a valuable measure of the analytical model's veracity at higher angles. A comparison of $(Cd_c)_h$ with Fig. 8 of Ref. 11 shows that the results are typical for supercritical cross flows, whose values range between 0.14 and 0.30 for the Reynolds numbers of the models tested. Likewise, the $(Cd_c)_f$ results are very representative of those in Fig. 86 of Ref. 7, whose values range from 2.0 to 4.0 for the geometries tested.

These comparisons are encouraging, in that the results for $(Cd_c)_h$ and $(Cd_c)_f$ are essentially functions of the second derivatives of the curve-fitted force and moment coefficients, which makes these much more susceptible to data error than η_k and η_f. In conclusion, then, the analytical model appears

Table 1 Characteristics of example airships used in least-squares matching of theory and experiment

Airship	CBV-250	CBV-350	ZR-1	ZRS-4	University of Washington
$\hat{S}_h$	1.0	1.0	1.0	1.0	1.0
$\hat{S}_f$	0.7617	0.6070	0.3692	0.4442	0.9358
$\hat{I}_1$	0.2329	0.1856	0.1079	0.2202	0.3119
$\hat{J}_1$	1.5193	1.6672	2.2446	1.8501	1.4450
$\hat{I}_3$	−0.2111	−0.2012	−0.0985	−0.0548	−0.0768
$\hat{J}_2$	0.6234	0.7127	0.9523	0.7629	0.5422
$(Cn^*_\alpha)_f$	2.3696	2.3696	1.2449	1.7733	1.8056
$(\hat{l}_f)_1$	0.9319	0.9463	0.8668	0.8131	0.7772
$(\hat{l}_f)_2$	1.0241	1.0190	0.9137	0.8644	0.8484
$(k_3 - k_1)$	0.624	0.723	0.924	0.870	0.731

Table 2 Results from least-squares matching of theory and experiment for example airships

Airship	CBV-250	CBV-350	ZR-1	ZRS-4	University of Washington
η_f	0.7536	0.6792	0.4094	0.2600	0.5720
η_k	1.3404	1.2150	1.0476	1.0497	1.2587
$(Cd_c)_f$	1.0903	2.0809	3.4014	3.2655	2.2514
$(Cd_c)_h$	0.2164	0.2380	0.2810	0.2125	0.1188
S_{fh}/S_f	0.1905	0.1905	0.4633	0.5699	0.3776
$S_f\cos^2(\Gamma)/(J_1)_{\text{tot}}$	0.4576	0.3405	0.1522	0.2062	0.3854

to give a good aerodynamic representation of finned axisymmetric bodies with attached flow.

Dynamic Model

The steady-state analytical model provides a framework for computing forces and moments when the vehicle is in unsteady motion, having an angular velocity, ω, with components, P, Q, R and a relative velocity at a reference point, V, with components U, V, W in the body-fixed coordinate system. There may also be a space- and time-dependent turbulence, $V_g(\xi,t)$, having components $(u,v,w)_g$. For this purpose the hull is divided into a number of vertical "slices" or panels and the fins are considered separate panels. The ith hull panel, extending from l_i to l_{i+1}, is shown by the shaded area in Fig. 1. The force on a panel is computed using the relations in Eqs. (1) and (2), taking into account the local relative velocity and angle of attack and assuming $(Cd_c)_h$ and $(k_3-k_1)\eta_k \equiv K$ remain constant along the length of the hull.

With reference to Fig. 4, consider the vertical section of the hull of thickness $d\xi$ with its center located at r in a body-fixed coordinate system having its origin at the center of rotation. The local components of relative velocity on the section are

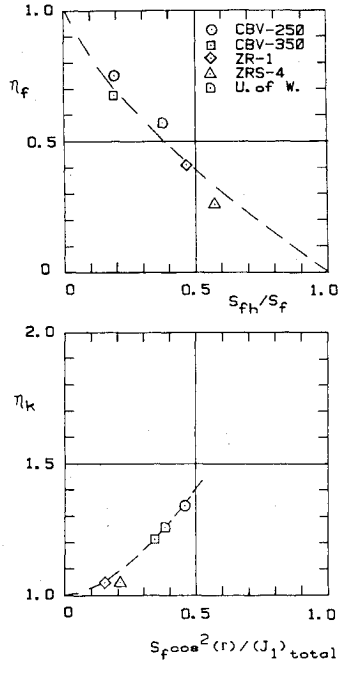

Fig. 3 Fin- and hull-efficiency factors from experimental data.

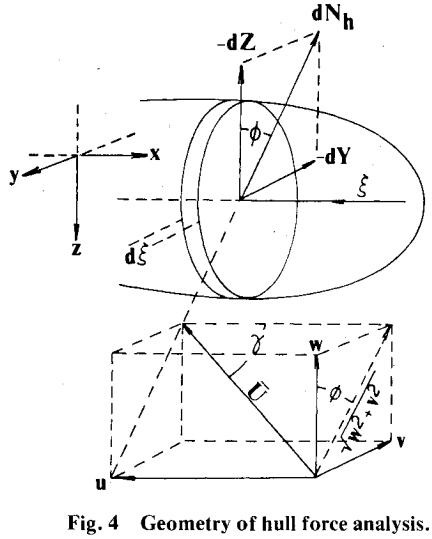

Fig. 4 Geometry of hull force analysis.

$$v = V + \omega \times r = \begin{Bmatrix} u = U + Qz - Ry \\ v = V + Rx - Pz \\ w = W + Py - Qx \end{Bmatrix} \tag{14}$$

Referring to Fig. 4, the normal force lies in the plane inclined at the angle ϕ, the local angle of attack is γ, and the local absolute velocity is $\bar{U}$.

$$\bar{U}^2 = u^2 + v^2 + w^2 \tag{15}$$

From Eq. (1), the normal force on the element is

$$dN_h = \tfrac{1}{2}\rho\bar{U}^2 [K\sin(2\gamma)\cos(\gamma/2)\frac{dA}{d\xi}d\xi + (Cd_c)_h \sin\gamma\sin|\gamma| 2r d\xi] \tag{16}$$

Resolving the normal force into components in the body coordinate system gives

$$dZ = -\cos\phi dN_h = dZ_a + dZ_c \tag{17}$$

$$dY = -\sin\phi dN_h = dY_a + dY_c \tag{18}$$

The subscripts a and c refer to the potential (attached) and cross-flow drag components of force, respectively. Considering the geometry of Fig. 4, the normal forces on an incremental element can be written in terms of the local flow.

$$\cos(\gamma/2) = \sqrt{\frac{\bar{U}+u}{2\bar{U}}} \tag{19}$$

$$dZ_a = -\rho K u w \sqrt{\frac{\bar{U}+u}{2\bar{U}}}\frac{dA}{d\xi}d\xi \tag{20}$$

$$dZ_c = -\rho(Cd_c)_h w\sqrt{w^2+v^2}\, r d\xi \tag{21}$$

$$dY_a = -\rho K u v \sqrt{\frac{\bar{U}+u}{2\bar{U}}}\frac{dA}{d\xi}d\xi \tag{22}$$

$$dY_c = -\rho(Cd_c)_h v\sqrt{w^2+v^2}\, r d\xi \tag{23}$$

For the sake of brevity, only the vertical forces will be considered. Let the center of rotation be l_0 from the nose, measured along the centerline. Now x in Eq. (14) is replaced by $x = l_0 - \xi$, while y and z are independent of ξ. The force on the ith panel is obtained by integrating Eqs. (20) and (21) from $\xi = l_i$ to l_{i+1}. This is facilitated by the following approximations valid for small panels.

$$(Z_a)_i = -\rho K \int_{l_i}^{l_{i+1}} uw\sqrt{\frac{\bar{U}+u}{2\bar{U}}}\frac{dA}{d\xi}d\xi \simeq -\rho K\sqrt{\frac{\bar{U}+u}{2\bar{U}}}\int_{l_i}^{l_{i+1}} uw\frac{dA}{d\xi}d\xi \tag{24}$$

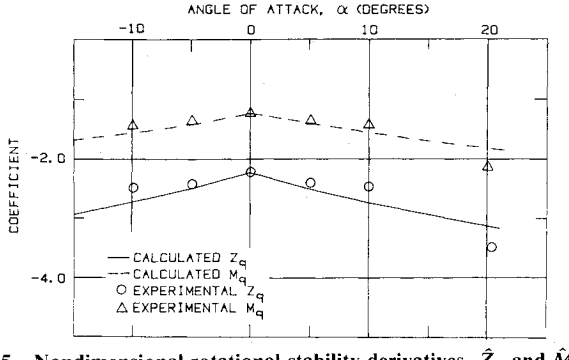

Fig. 5 Nondimensional rotational stability derivatives, $\hat{Z}_q$ and $\hat{M}_q$, for the TCOM 250 aerostat, calculated from theory and measured in a rotating-arm water tow tank.

$$(Z_c)_i = -\rho(Cd_c)_h \int_{l_i}^{l_{i+1}} w\sqrt{w^2+v^2}\,r\,d\xi$$

$$\simeq -\rho(Cd_c)_h \sqrt{1+(v/w)^2} \int_{l_i}^{l_{i+1}} w|w|r\,d\xi \quad (25)$$

When the integrations are carried out over a panel, for the vertical force one obtains,

$$(Z_a)_i = -\rho K f_a(\bar{U},u)_i u[(W+Py)(I_1)_i - G_1(l_0)_i Q] \quad (26)$$

$$(Z_c)_i = -\rho\frac{(Cd_c)_h}{2} f_c(w,v)_i [(W+Py)^2(J_1)_i - 2(W+Py)H_1(l_0)_i Q + H_2(l_0)_i Q^2] \quad (27)$$

where

$$f_a(\bar{U},u) = \cos(\gamma/2) = \sqrt{(\bar{U}+u)/2\bar{U}} \quad (28)$$

$$f_c(w,v) = \sqrt{1+(v/w)^2}\,\mathrm{sgn}(w) \quad (29)$$

Sgn(w) is unity with the algebraic sign of w.

$$G_1(l_0) = l_0 I_1 - I_3 \quad (30)$$

$$G_2(l_0) = l_0^2 I_1 - 2l_0 I_3 + I_5 \quad (31)$$

$$H_1(l_0) = l_0 J_1 - J_2 \quad (32)$$

$$H_2(l_0) = l_0^2 J_1 - 2l_0 J_2 + J_3 \quad (33)$$

$$H_3(l_0) = l_0^3 J_1 - 3l_0^2 J_2 + 3l_0 J_3 - J_4 \quad (34)$$

The list of hull integrals introduced previously must be expanded as follows:

$$I_{2j-1} = \int \xi^{j-1}\frac{dA}{d\xi}d\xi \quad (35)$$

$$I_{2j} = \int \xi^{j-1} A\,d\xi \quad (36)$$

$$J_j = \int 2r\xi^{j-1}d\xi \quad (37)$$

The subscript i in Eqs. (26) and (27) indicates that the integrals are taken over a panel.

Additional normal forces on the hull result from inertia due to accelerations and rotations.[3] Considering the local flow to be constant over a panel, these forces are

$$dZ_I = -\rho[k_3'\dot{w} - k_1'Qu + k_2'Pv]A\,d\xi \quad (38)$$

The k' values are the Munk constants modified for hull-fin interference such that

$$k_3' - k_1' = (k_3 - k_1)\eta_k \quad (39)$$

The η_k distribution is assumed to be constant. This is based on results in Ref. 11 which show that the distributed normal force along a body is reasonably calculated by using the body's overall $k_3 - k_1$ parameter as the coefficient at any given station. However, the relatively low fineness ratios of typical aerostats compel further study of this assumption.

In order to integrate Eq. (38) the velocity and acceleration terms must be expanded. The former are given by Eqs. (14) and the time rate of change of relative velocity in the body frame of reference is

$$\dot{v} = \dot{V} + \dot{\omega}\times r + \omega\times\dot{r} \quad (40)$$

The last term on the right is the convective acceleration which arises from the fact that the fluid motion is Eulerian. In other words, r must be regarded as the radius vector of a fluid particle which moves relative to the body frame and coincides with a fixed point at the instant considered. In terms of body motion relative to the fluid,

$$\dot{r} = -v \quad (41)$$

$$\dot{v} = \dot{V} + \dot{\omega}\times r - \omega\times v \quad (42)$$

This can also be written in the more familiar form,

$$\frac{dv}{dt} = \left[\frac{\partial}{\partial t} - u\frac{\partial}{\partial x} - v\frac{\partial}{\partial y} - w\frac{\partial}{\partial z}\right]v \quad (43)$$

While Eq. (42) is the strict definition of acceleration of the body relative to the fluid, its application to Eq. (38) can be questioned. The latter is based on Munk's assumption that apparent mass can be treated as a rigid body,[17] to which the convective acceleration would not apply. On the other hand, Munk found it necessary to assume it has an Eulerian character in order to derive the potential force. Referring to the area of apparent mass transverse to the axis, he employs the following relation[18]:

$$\frac{\partial A}{\partial t} = \frac{\partial A}{\partial \xi}\cdot\frac{\partial \xi}{\partial t} = \frac{\partial A}{\partial \xi}u$$

Note that

$$\frac{\partial \xi}{\partial t} = u$$

which is equivalent to Eq. (41). The same concept is used by Logvinovich,[19] who derived the potential and inertial force using a "pierced layer" model. Calligeros and McDavitt[20] have shown that turbulence in the form of a traveling wave or gust front propagated at the velocity, U, does not contribute to the inertial force since

$$\frac{d}{dt}V_g(\xi,t) = \left[\frac{\partial}{\partial t} + U\frac{\partial}{\partial \xi}\right]V_g = 0 \quad (44)$$

Clearly, this is an expression of the acceleration in Eulerian coordinates including the local and convective terms.

Additional evidence that the convective terms of Eq. (42) are applicable to the inertial force is provided by experimental data from a rotating-arm tow tank, which will be presented in the next section. In that case the angle of attack and angular velocity were constant; therefore local acceleration was absent but there was convective acceleration. Only if the latter is included in Eq. (38) do theoretical calculations agree well with the experimental data.

Using Eq. (42), the vertical component of acceleration is

$$\dot{w} = \dot{W} + \dot{P}y - \dot{Q}x - Pv + Qu \quad (45)$$

When this is substituted in Eq. (38) one obtains

$$dZ_I = -\rho[k_3'(\dot{W} + \dot{P}y - \dot{Q}x) + (k_3' - k_1')Qu + (k_2' - k_3')Pv]A\,d\xi \quad (46)$$

Assuming an axisymmetric body in which $k_3' = k_2'$ and integrating, the inertial force on a panel is found:

$$(Z_I)_i = -\rho[k_3'(\dot{W} + \dot{P}y) + KQu](I_2)_i + \rho k_3'\dot{Q}(l_0 I_2 - I_4)_i \quad (47)$$

The normal forces due to the horizontal fins, expressed in terms of the local relative velocities, are

$$(Z_a)_f = -(\rho/2)(Cn_\alpha^*)_f \eta_f S_f u(W + Py - \lambda_i Q) \quad (48)$$

$$(Z_c)_f = -(\rho/2)(Cd_c)_f S_f \mathrm{sgn}(w_f)(W+Py-\lambda_2 Q)^2$$

$$= -(\rho/2)(Cd_c)_f S_f \mathrm{sgn}(w_f)[(W+Py)^2$$

$$-2(W+Py)\lambda_2 Q+\lambda_2^2 Q^2] \quad (49)$$

where

$$\lambda_1,\lambda_2 = l_0-(l_f)_1, l_0-(l_f)_2$$

The force on the horizontal fin due to acceleration, $\dot{w}_f$, has been treated by DeLaurier,[21] who considered the components due to apparent mass and shed vorticity. These effects are both functions of fin aspect ratio but are opposite in sign. At an aspect ratio of approximately 3, which is typical for airships and aerostats, the effects cancel and can be ignored.

In the above formulations the local flow may contain a component of turbulence, in which case

$$v_i = v+(V_g)_i$$

$$w_i = w+(W_g)_i$$

However, in view of Eq. (44), if the turbulence is in the form of a traveling wave it does not contribute to the inertial force.

The total force is obtained by summing the panel forces.

$$Z=\sum_1^n [(Z_a)_i+(Z_c)_i+(Z_I)_i]+(Z_a)_f+(Z_c)_f \quad (50)$$

The drag force can be distributed on the panels by extracting the potential and cross-flow drag components for the hull and fins from Eq. (2).

The moments due to the normal forces on a hull panel are obtained from

$$(M)_i = -\int_{l_i}^{l_{i+1}} (l_0-\xi)[\mathrm{d}(Z_a)_i+\mathrm{d}(Z_c)_i+\mathrm{d}(Z_I)_i] \quad (51)$$

and for the horizontal fin from

$$(M)_f = -(Z_a)_f\lambda_1-(Z_c)_f\lambda_2 \quad (52)$$

The results are

$$(M_a)_i = \rho K f_a(\bar{U},u)_i u[(W+Py)G_1(l_0)_i - G_2(l_0)_i Q] \quad (53)$$

$$(M_c)_i = [\rho(Cd_c)_h/2] f_c(w,v)_i [(W+Py)^2 H_1(l_0)_i$$

$$-2(W+Py)H_2(l_0)_i Q+H_3(l_0)_i Q^2] \quad (54)$$

$$(M_I)_i = \rho\{k_3'[(\dot{w}+\dot{P}y)(l_0 I_2-I_4)_i - \dot{Q}(l_0^2 I_2-2l_0 I_4+I_6)_i]$$

$$+KQu(l_0 I_2-I_4)_i\} \quad (55)$$

$$(M_a)_f = [\rho(Cn_\alpha^*)_f/2]\eta_f S_f u[(W+Py)\lambda_1-\lambda_1^2 Q] \quad (56)$$

$$(M_c)_f = [\rho(Cd_c)_f/2] S_f \mathrm{sgn}(w_f)[(W+Py)^2\lambda_2$$

$$-2(W+Py)\lambda_2^2 Q+\lambda_2^3 Q^2] \quad (57)$$

The total pitching moment is then

$$M=\sum_1^n [(M_a)_i+(M_c)_i+(M_I)_i]+(M_a)_f+(M_c)_f+zX \quad (58)$$

where X is the total axial drag obtained from Eq. (2) or summed over the panels.

Computation of Rotational Stability Derivatives

Rotational stability derivatives result from the polynomial representation of the functional relation between force or moment and angular velocity. Thus, for the vertical force,

$$Z = Z_0+Z_q Q+Z_{qq}Q^2+\ldots \quad (59)$$

The equations for force and moment derived above are quite general and can be used for the entire hull if the angle of attack is small and there is no lateral component of velocity such that

$$f_a(\bar{U},u)=1$$

$$f_c(w,v)=\mathrm{sgn}(w)$$

The stability derivatives Z_q and M_q are obtained from Eqs. (50) and (58). Neglecting terms containing Q^2, one obtains

$$Z_q = \frac{\partial Z}{\partial Q} \quad (60)$$

$$M_q = \frac{\partial M}{\partial Q} \quad (61)$$

For Z_q the result is

$$Z_q = \rho U_0\{KG_1(l_0)-KI_2+[(Cn_\alpha^*)_f/2]\eta_f S_f\lambda_1\}\cos\alpha$$

$$+\rho U_0[(Cd_c)_h H_1(l_0)+(Cd_c)_f S_f\lambda_2]\,|\sin\alpha| \quad (62)$$

where

$$U_0\cos\alpha = U \qquad U_0\sin\alpha = W$$

In nondimensional form one obtains

$$\hat{Z}_q = \{4K[\hat{G}_1(\hat{l_0})-\hat{I}_2]+2(Cn_\alpha^*)_f\eta_f\hat{S}_f\hat{\lambda}_1\}\cos\alpha$$

$$+4[(Cd_c)_h\hat{H}_1(\hat{l_0})+(Cd_c)_f\hat{S}_f\hat{\lambda}_2]\,|\sin\alpha| \quad (63)$$

$$\hat{M}_q = -\{4K[\hat{G}_2(\hat{l_0})-(\hat{I}_2\hat{l_0}-\hat{I}_4)]$$

$$+2(Cn_\alpha^*)_f\eta_f\hat{S}_f\hat{\lambda}_1^2\}\cos\alpha$$

$$-4[(Cd_c)_h\hat{H}_2(\hat{l_0})+(Cd_c)_f\hat{S}_f\hat{\lambda}_2^2]\,|\sin\alpha| \quad (64)$$

where

$$Q=\hat{Q}(2U_0/\bar{C})$$

$$Z_q=\hat{Z}_q(\rho U_0 S\bar{C}/4)$$

$$M_q=\hat{M}_q(\rho U_0 S\bar{C}^2/4)$$

$$l_0,\lambda_1,\lambda_2=(\hat{l_0},\hat{\lambda}_1,\hat{\lambda}_2)\bar{C}$$

$$G_j,H_j,I_{2j}=(\hat{G}_j,\hat{H}_j,\hat{I}_{2j})S\bar{C}^j$$

$$I_{2j-1},J_j=(\hat{I}_{2j-1},\hat{J}_j)S\bar{C}^{j-1}$$

The rotational stability derivatives have been measured experimentally for the TCOM 250 aerostat using a rotating-arm water tow tank.[22] This provides data for comparison of Eqs. (63) and (64), which employ data obtained from static wind tunnel tests, with experimental dynamic tests. In the tow-tank experiments, $\hat{Q}$ was sufficiently small that the effects of $\hat{Q}^2$ can be neglected and the results can be compared directly with the theory. These comparisons for $\hat{Z}_q$ and $\hat{M}_q$ are shown in Fig. 5.

The hull integrals and geometric data for this aerostat not included in Tables 1 and 2 are given below.

$$\hat{I}_0 = 0.2708$$

$$\hat{I}_2 = 0.40506$$

$$\hat{I}_4 = 0.16253$$

$$\hat{G}_1(\hat{I}_0) = 0.27436$$

$$\hat{G}_2(\hat{I}_0) = -0.03233$$

$$\hat{J}_3 = 0.33186$$

$$\hat{H}_1(\hat{I}_0) = -0.58238$$

$$\hat{H}_2(\hat{I}_0) = 0.00530$$

The agreement of theory with experiment is particularly good at low angles of attack, being about 1% deviation at $\alpha = 0$, for both $\hat{Z}_q$ and $\hat{M}_q$. It should be noted that the acceleration term derived from Eq. (47), which does not include a contribution due to the fin, is a significant part of $\hat{Z}_q$. The agreement of theory with experiment supports the prediction of DeLaurier[21] that the fin force due to acceleration can be ignored.

Summary and Conclusions

A steady-state, attached-flow analytical model based on Allen and Perkins[2] for the hull and Wardlaw[7] for the fins has been refined by the introduction of efficiency factors η_k and η_f. These factors account for the effect of the fins on the hull and the hull on the fins, respectively. Wind tunnel data on five airships and aerostats have been analyzed in the context of the model to obtain semiempirical values of these factors as well as the cross-flow drag coefficients for the hull and fins. The latter agree well with the data of Wardlaw[7] and Putman et al.,[11] providing a measure of the veracity of the model.

The fin-efficiency factor, η_f, shows a logical trend between 1.0 and 0 when plotted against the ratio of the fin area submerged in the hull to the total fin area. The hull efficiency factor, η_k, increases from unity as the ratio of fin area to hull projected area increases.

The model is extended to unsteady motion by considering the local relative velocities on the fins and elements of the hull. For dynamic simulations a "panel" model is derived in which force and moment can be computed for finite vertical "slices" of the hull, taking into account potential, cross-flow drag, and inertial components.

For low angles of attack and $\beta = 0$ the panel model can be generalized to the fins and a single hull panel, permitting the computation of rotational stability derivatives from static data. For one aerostat a comparison of calculated Z_q and M_q with experimental values obtained in a rotating-arm water tow tank gives good agreement at low angles of attack.

References

[1] Munk, M.M., "Aerodynamics of Airships," *Aerodynamic Theory,* Vol. 6, Durand, W.F., ed., Julius Springer, Berlin, 1936, pp. 32-48.

[2] Allen, H.J. and Perkins, E.W., "A Study of Viscosity on Flow Over Slender Inclined Bodies of Revolution," NACA Report 1048, 1951.

[3] Jones, R., "Acceleration Derivatives in the Case of a Body Moving in an Ideal Fluid," ARC R&M 748, April 1921.

[4] Multhopp, H., "Aerodynamics of the Fuselage," NACA TM 1036, 1942.

[5] Nielsen, J.N., "Stability Derivatives," in *Missile Aerodynamics,* McGraw-Hill, New York, 1960, pp. 349-420.

[6] DeLaurier, J. and Podleski, S., "A Semi-Empirical Method for Estimating the Subsonic Aerodynamic Characteristics of Finned Axisymmetric Bodies," *Proceedings of the Tenth AFGL Scientific Balloon Symposium,* Air Force Geophysics Laboratory, March 1, 1979, pp. 461-487.

[7] Wardlaw, A.B., "High-Angle-of-Attack Missile Aerodynamics," in *Missile Aerodynamics,* AGARD Lecture Series 98, Feb. 1979, pp. (5-1), (5-53).

[8] Etkin, B., "Lift-Curve Slope, Cl_α," in *Dynamics of Flight,* 5th ed., John Wiley and Sons, New York, 1966, pp. 446-447.

[9] Lowry, J. G. and Polhamus, E., "A Method for Predicting Lift Increments Due to Flap Deflection at Low Angles of Attack in Incompressible Flow," NACA TN 3911, 1957.

[10] Hoerner, S.F., *Fluid-Dynamic Drag,* published by the author, Midland Park, N.J., 1965.

[11] Putman, W.F., Maughmer, M., Curtiss, H.C., and Traybar, J.J., "Aerodynamics and Hovering Control of LTA Vehicles," Department of Aerospace and Mechanical Sciences, Princeton University, Princeton, N.J., AMSTR 1339, May 1977.

[12] Gove, T.B. and Haak, E.L., "MK VII and MK VII-S Wind Tunnel Study," Sheldahl, Inc., SER 0185, May 1974.

[13] Zahm, A.F., Smith, R.H., and Louden, F.A., "Air Forces, Moments and Damping on Model of Fleet Airship Shenandoah," NACA Report 215, 1925.

[14] Freeman, H.B., "Force Measurements on a 1/40-Scale Model of the U.S. Airship 'Akron'," NACA Report 432, 1932.

[15] Peters, P.A., Lysons, H.H., and Shindo, S., "Aerodynamic Coefficients of Four Balloon Shapes at High Attack Angles," *Proceedings of the Seventh AFCRL Scientific Balloon Symposium,* Air Force Cambridge Research Laboratories, Jan. 3, 1973, pp. 19-47.

[16] Purser, P.E. and Campbell, J.P., "Experimental Verification of a Simplified Vee Tail Theory, and Analysis of Available Data on Complete Models with Vee-Tails," NACA TR 823, 1945.

[17] Munk, M.M., "Motion of Solids in a Fluid," *Aerodynamic Theory,* Vol. 1, Durand, W.F., ed., Julius Springer, Berlin, 1934, pp. 241-248.

[18] Munk, M.M., "Lateral Motion of Surfaces of Revolution," in *Aerodynamic Theory,* Vol. 1, Durand, W.F., ed., Julius Springer, Berlin, 1934, pp. 269-276.

[19] Logvinovich, G.V., "Hydrodynamics of Free-Boundary Flows," NASA TT F-658, 1972, pp. 134-147.

[20] Calligeros, J.M. and McDavitt, P.W., "Response and Loads on Airships Due to Discrete and Random Gusts," Bureau of Aeronautics, Department of the Navy, Contract No. 56-825-6, MIT Technical Report 72-1, Feb. 1958.

[21] DeLaurier, J.D., "Refinements and Experimental Comparisons of a Stability Analysis for Aerodynamically-shaped Tethered Balloons," AIAA 75-943, July 1975.

[22] Strumpf, A., "Rotating-Arm Model Experiments of Two TCOM Aerostats Tested With and Without Appendages," Davidson Laboratory Report, SIT-DL-78-9-2027, TCOM Corporation, Columbia, Md., Dec. 1978.